



Bone Marrow Mesenchymal Stem Cell Condition Medium Loaded on PCL Nanofibrous Scaffold Promoted Nerve Regeneration After Sciatic Nerve Transection in Male Rats

Amir Raoofi^{1,2,3} · Yousef Sadeghi⁴ · Abbas Piryaei⁵ · Ensieh Sajadi⁵ · Abbas Aliaghaei⁵ · Ali Rashidiani-Rashidabadi⁶ · Fatemeh Fadaei Fatabadi⁵ · Behnam Mahdavi⁷ · Mohammad-Amin Abdollahifar^{3,5} · Amin Mousavi Khaneghah⁸

Received: 25 March 2021 / Revised: 29 June 2021 / Accepted: 1 July 2021 / Published online: 26 July 2021
© The Author(s), under exclusive licence to Springer Science+Business Media, LLC, part of Springer Nature 2021

Abstract

Nowadays, researchers pay a vast deal of attention to neural tissue regeneration due to its tremendous effect on the patient's life. There are many strategies, from using conventional autologous nerve grafts to the newly developed methods for reconstructing damaged nerves. Among the various therapeutic methods, incorporating highly potent biomolecules and growth factors, the damaged nerve site would promote nerve regeneration. The aim was to examine the efficiency of a mesenchymal stem cell condition medium (MSC-CM) loaded on a 3D-polycaprolactone (PCL) scaffold as a nerve conduit in an axotomy rat model. Twenty-four mature male rats were classified into four groups: controls (the animals of this group were intact), axotomy (10 mm piece of the nerve was removed), axotomy (10-mm piece of the nerve was removed) + scaffold, and axotomy (10-mm piece of the nerve was removed) + MSC-CM-loaded scaffold. We followed up nerve motor function using a sciatic function index and electromyography activity of the gastrocnemius muscle. At 12 weeks post axotomy, sciatic nerve and dorsal root ganglion specimens and L4 and L5 spinal cord segments were separated from the rats and were analyzed by stereological, immunohistochemistry, and RT-PCR procedures. The rats of the axotomy group presented the expected gross locomotor deficit. Stereological parameters, immunohistochemistry of GFAP, and gene expression of S100, NGF, and BDNF were significantly enhanced in the CM-loaded scaffold group compared with the axotomy group. The most observed similarity was noted between the results of the control group and the CM-loaded scaffold group. Our results support the potential applicability of MSC-CM-loaded PCL nanofibrous scaffold to treat peripheral nerve injury (PNI).

Keywords Peripheral axotomy · Axonal regeneration · Bone marrow mesenchymal stem cells · PCL scaffold

✉ Mohammad-Amin Abdollahifar
m_amin58@yahoo.com; abdollahima@sbmu.ac.ir;
mabdollahifar1360@gmail.com

¹ Leishmaniasis Research Center, Sabzevar University of Medical Sciences, Sabzevar, Iran

² Department of Anatomy, Sabzevar University of Medical Sciences, Sabzevar, Iran

³ Hearing Disorders Research Center, Loghman Hakim Medical Center, Shahid Beheshti University of Medical Sciences, Tehran, Iran

⁴ Department of Anatomy and Neuroscience, Faculty of Medicine, Dentistry and Health Science, University of Melbourne, Melbourne, VIC, Australia

⁵ Department of Biology and Anatomical Sciences, School of Medicine, Shahid Beheshti University of Medical Sciences, Tehran, Iran

⁶ Department of Anatomical Sciences, Lorestan University of Medical Sciences, Khorramabad, Iran

⁷ Department of Chemistry, Faculty of Science, Hakim Sabzevari University, Sabzevar, Iran

⁸ Department of Food Science and Nutrition, Faculty of Food Engineering, University of Campinas (UNICAMP), Campinas, São Paulo, Brazil

Introduction

Axotomy of peripheral nerve injury is caused by trauma and medical disorders (Grinsell and Keating 2014). Severe nerve injury has a devastating impact on a patients' quality of life. Typical symptoms are sensory and motor function defects that can result in complete paralysis of the affected limb or the development of intractable neuropathic pain (Siemionow and Brzezicki 2009). Following peripheral axotomy, some of the dorsal root ganglion (DRG) and ventral horn neurons undergo a series of retrograde degenerative changes that lead to neuronal death (Himes and Tessler 1989, Vestergaard et al. 1997, Terenghi 1999, Pierucci and de Oliveira 2006). The degenerative changes of neurons are made by damage-induced interruption of the flow of neurotrophic factors from the perimeter to the neuronal body by retrograde transport (Terenghi 1999). Albeit three different types of grafts, including autografts, allografts, and xenografts, were used for nerve regeneration, they possess disadvantages including immunological rejection (in cases of allografts and xenografts) and finite availability (Kim et al. 2006a; Zalewski and Gulati 1981). Currently, no effective strategies to better neural tissue regeneration were introduced. Thus, the development of artificial nerve grafts is needed.

Electrospun nanofibers were investigated as a scaffold for regeneration and repair in neural tissue applications. Specifically, aligned nanofibers are more suitable for neurite development than haphazardly oriented nanofibers because the alignment provides a guidance queue, and the anatomical features of normal nerves are highly organized and aligned (Lee et al. 2005; Schnell et al. 2007). Polycaprolactone or PCL is a semi-crystalline-linear-hydrophobic polymer. Though the electrospun PCL mats mimic the identity of ECM in living tissues, its poor hydrophilicity caused a reduction in the ability of cell adhesion, migration, proliferation, and differentiation (Kim et al. 2006b; Li et al. 2006).

On the other hand, natural biopolymers, because of their excellent merits, such as their biological origin, biodegradability, and biocompatibility, were widely used in the pharmaceutical and medical fields (Chong et al. 2007). Accordingly, natural biomolecules such as proteins and growth factors can be blended with synthetic ones to obtain a scaffold with desired cell adhesion, degradation, and neural regeneration (Koh et al. 2008). It is well known that only a tiny percentage of motoneurons can successfully achieve regeneration, and new treatments are necessary to improve such rates. In this sense, MSC therapy is a promising approach. MSC can modify the pro-inflammatory response, reduce the inhibitory effects of the glial scar, and promote a permissive environment for axonal extension. They may also provide growth factors that contribute to cell

survival and axonal elongation (Wright et al. 2011). Undifferentiated MSCs showed a positive influence on neurite outgrowth in vitro, indicating that these cells can express a wide range of growth factors, especially neurotrophic factors (Ladak et al. 2011). Due to the properties described above, the MSC was proposed as a promising tool for treating lesions (Morales 2007). Although mesenchymal stem cell transplantation was successful, the immunogenicity of these cells and the need to suppress the recipient's immune system were reported, which resulted in introducing paracrine secretions from these cells rather than the cell itself a safe and low-risk treatment (Griffin et al. 2010). In the present study, optimum MSC-condition medium (CM) was coated on the surface of the PCL scaffold, and the sciatic nerve repair was investigated using the prepared scaffold after axotomy.

Material and Method

Rat BM-MSc Cultivation and Conditioned Media Preparation

BM-MSc Isolation and Purification

The Medical Ethics Committee approved the entire procedure of Shahid Beheshti University of Medical Sciences (Tehran, Iran; Protocol No. 5137). Bone marrow-derived mesenchymal stem cells were harvested from 28-day-old male Wistar rats. Briefly, the rats were sacrificed, the humerus and tibias were dissected in sterile conditions and placed in a petri dish containing DMEM (Bio-Idea Company, Iran) media with antibiotics. The bone metaphysis was cut, and bone marrow tissue was carefully collected by flushing complete media. The bone marrow suspensions were filtered through a 70- μ m nylon cell strainer into a 75cm² flask (SPL, Korea). The cell-culture flasks were incubated at the humidified 37 °C and 5% CO₂ concentration. Non-adherent cells were removed from the culture after 48 h of cell seeding by a series of washes in PBS and subsequent medium changes. The culture medium was refreshed every 2–3 days until the flask attained 80% confluency. Before being used, the MSCs had been expanded for 3 passages (P3) and characterized (Karaoz et al. 2009).

Immunophenotyping of Cultured BM-MSCs by Flow Cytometry

The flow cytometry was performed to determine the purity of MSCs. Cultured P3 MSCs trypsinized and pelleted, then were fixed for 10 min at 4% formaldehyde solution (Merck, Germany). Cells were then washed with PBS (Gibco, UK) containing 5% Tween (Merck, Germany). After the cells

were incubated with 2% bovine serum albumin (Sigma, USA) blocking solution for 20 min, the cells were incubated with fluorescence isothiocyanate (FITC)- or PE-conjugated primary polyclonal antibody against positive mesenchymal markers and negative markers like CD-44, CD-90, and CD-34, and CD-45 respectively at room temperature for 40 min. Isotype antibodies were used as negative controls. Eventually, the results were evaluated with a flow cytometer, and data were analyzed using WinMDI software (Becton–Dickinson, San Jose, CA, USA).

Osteogenic Differentiation

P3 cells were counted and seeded on 6-well tissue culture plates at 6000 cells/well. After achieving 80% confluence, the growth medium was replaced with an osteogenic induction medium (Stem pro-Gibco), whereas other wells supplemented with a complete medium served as a negative control. The medium was changed every 2 to 3 days and maintained up to 21 days. On day 21, the cells were fixed for 10 min with 4% formaldehyde solution, and the differentiation potential of osteogenesis was evaluated by 20 mg/ml Alizarin Red staining (Sigma-Aldrich) pH 4.2 for 30 min for mineral calcium deposition. Calcium depots were visualized by light microscopy (Pittenger et al. 1999).

Adipogenic Differentiation

Adipogenesis was induced by culturing the bone marrow mesenchymal stem cells (BM-MSCs) with an adipogenic induction medium. P3 cells were plated onto 6-well plates at 6000 cells/cm², as previously reported. After attaining 80% confluence, the growth medium was replaced with an adipogenic induction medium (Stem pro/Gibco). The medium was maintained for up to 3 weeks, and the media was changed twice weekly. The cells were fixed with 10% formaldehyde (Sigma-Aldrich). The presence of intracellular lipid-rich vacuole indicated it positive for adipogenic differentiation, which was confirmed by Oil Red O staining (500 µl/well, Sigma-Aldrich; 3.5 g/l in isopropanol, mixed 3:2 with double-distilled water) for 10 min, following the manufacturer's protocol and taking micrographs with a light microscope (Pittenger et al. 1999).

Preparation of BM-MSC CM

After ensuring that cells are compatible, preparation of CM was done in a single stage. In the current study, CM was prepared by culturing passage-4 BM-MSCs in a T75-culture flask, and cells were grown until they were approximately 80% confluent. Cells were then washed twice with a phosphate buffer solution (PBS). The complete media were changed with a serum-free basal medium and incubated for

48 h at 37 °C. The CM was extracted and concentrated to tenfold by lyophilized drying (Christ Alpha1-2 LD Plus, Germany), and then the CM was cryopreserved at –20 °C up to the use (Ganji et al. 2014).

Western Blot

Western blot analysis was conducted for detection of vascular endothelial growth factor (VEGF) of MSCs. Briefly, after washing in PBS solution, the total protein of MSC lysate was extracted using whole-cell radioimmunoprecipitation assay (RIPA) lysis buffer (Beyotime Inc., Nanjing, China) centrifuged at 12,000 rpm for 10 min at 4 °C. Next, to measure the concentration of total protein in the samples, Bradford's method was applied. Sixty micrograms of protein sample was loaded on SDS-PAGE with 12% gels and transferred proteins electrophoretically onto the PVDF membrane (Millipore Co., Billerica, MA, USA). Following the transfer, the nonspecific binding of blots was blocked by immersing the membrane in 5% non-fat dry milk at room temperature for 1 h. Then the membrane was incubated overnight at 4 °C with anti-VEGF and anti-GAPDH antibodies (1:1000 monoclonal; Abcam). After washing the membrane with TBS, the membrane was incubated with HRP-labeled goat anti-rabbit secondary antibody (1:5000; Santa Cruz Biotechnology, USA) for 2 h at room temperature and, finally, immunoreactivity of polypeptides was detected using an ECL solution.

Fabrication of Scaffold

Polycaprolactone nanofibrous mat was made by electrospinning procedure. To sum up, Polycaprolactone (MW = 80 kDa) solution was procured in a specific solvent system containing acetic acid/formic acid. Following the overnight shaking, the procured polymer solution was placed in a 5 ml glass syringe and then loaded in the syringe pump of the electrospinning mechanism. Notably, electrospinning was run towards a rotating mandrel.

BM-MSC-CM Loading

At the second step, prepared BM-MSC conditioned media (CM) were coated on the nanofibers using plasma treatment. Briefly, the electrospun mat was located in the plasma chamber and treated by discharge plasma. Immediately after plasma treatment, BM-MSC conditioned media were added to the mat dropwise, and treated samples were allowed to react overnight at 4. Finally, CM-coated mats were cut into 1.4 2cm specimens wrapped around the 1cm nerve gap site by fixing their distal and proximal parts. Samples were sterilized by UV radiation before being used for in vitro and in vivo experiments.

Scanning Electron Microscope Observations

According to the research design, a morphological description of the resulting structure was performed with a scanning electron microscope (VEGA, SEM, & TESCAN, Czech). In addition, the average diameters of the electrospun fibers were estimated via measurement of 25 fibers in each specimen from the SEM micrographs with the help of the image analysis software (Image J™, NIH, MD, USA).

In Vitro Evaluation

L929 Cell Culture

The present research utilized the L929 mouse fibroblast cell line to do in-vitro assays. Therefore, the cells were cultured in RPMI 1640 medium containing 10% FBS, 1% penicillin/streptomycin, and 1% L-glutamine in the T-75-flask tissue culture. Then, the cells between four and six passages were exploited in the tests. Afterward, they were kept at 37, 5% CO₂, 95% air. This culture medium was refreshed every 3 days. Of course, the fibroblast cells were harvested at the confluence, then sub-cultivated in a similar medium. Finally, 0.05% trypsin/EDTA was used to dissociate the cells. Afterward, the cells were centrifuged and re-suspended in the medium before use.

Cytotoxicity Test

According to the research design, indirect cytotoxicity experiments using L929 mouse fibroblast cell line were used to examine probable release of the cytotoxic materials from the samples. In order to achieve the extracts, sterilized samples were submerged in the DMEM medium complemented with 1% penicillin/streptomycin and 10% FBS. Moreover, the non-interfered complete medium was regarded for preparing the controls. In addition, 24 h before the addition of the CM, L929 cells were seeded (cell density = 2 cells/well) in the 96-well tissue culture plate. Following incubation for 1 and 4 days, the extracts and the non-interfered media were removed, and then replaced with the medium of the preseeded cells. Of course, 3 replicates were regarded for all eluates and media. When 24 h passed, all wells' culture media were replaced with 150 µl solution, and incubation of the plate continued for 4 h. Then, 100 µl from the solution of each of the wells was transported to a 96-well plate. Afterward, the absorbance was measured in the wavelength of 570 nm

by the Thermo Scientific Multiscan Spectrum plate reader. Results were provided as the relative ratio of sample values to the control ones.

Animals and Surgical Procedures

Twenty-four adults male Wistar rats weighing approximately 260 g were used, and the rats were housed individually in standard cages 20 × 20 × 40 cm in size in a standard animal home (12h light/12h dark environment) water ad libitum. The rats were randomized into four groups (n = 6): (1) control group: healthy rats without any injuries, (2) axotomy group: rats with injured sciatic nerve without treatment, rats with axotomy engrafted by (3) PCL scaffold, or (4) PCL scaffold loaded by MSC-conditioned medium (scaffold + CM).

Briefly, for axotomy, the animals were anesthetized by intraperitoneal injection of sodium pentobarbital (40 mg/kg body weight) before the sciatic nerve was exposed by making a 2cm longitudinal skin incision then interrupted in the position 0.5 cm below ischial tuberosity in the right lateral thigh. The nerve segment (10 mm) was removed in the 3rd and 4th groups; the sciatic nerve defect was bridged by PCL scaffold or PCL scaffold + CM. After surgery, the animals in all groups were housed in their cages and fed routinely under normal conditions.

Sciatic Function Index

After 4, 8, and 12 weeks post-surgery, the walking pattern of animals was recorded to analyze the sciatic functional index (SFI) as described previously. Briefly, the rats were trained a few pre-experiments to walk down a wooden track (100 × 20 × 15 cm) into a darkened goal box. After surgery, the animal's hind paws were dipped using an ink pad, and the changes in their paw prints that resulted from nerve lesion and denervation were recorded. The recordings continued until five measurable footprints were collected. From the footprints, the following parameters were calculated using a ruler: print length (PL) that refers to the distance from the heel to the top of the third toe, intermediary toe spread (ITS) that refers to the distance from the second to the fourth toe, and toe spread (TS), the distance between the first and the fifth toe. All these measurements were obtained both from the right experimental foot (EPL, ETS, and EITS, respectively) and from the left non-operated foot (NPL, NTS, and NITS, respectively) of each rat. By using these data, SFI was calculated by the following equation (Bain et al. 1989):

$$\text{SFI} = -38.3 (\text{EPL} - \text{NPL}) / \text{NPL} + 109.5 (\text{ETS} - \text{NTS}) / \text{NTS} + 13.3 (\text{EIT} - \text{NIT}) / \text{NIT} - 8.8$$

Table 1 Sequence of primers used in RT-PCR

Gene	Sequence	Sequence primer	Product size (bp)
<i>Bdnf</i>	F	AAACCATAACCCCGCACACTC	156 bp
	R	AGCCTTCATGCAACCGAAGT	
<i>Ngf</i>	F	AAGAGAGCCTGGAGTGAGGGAT	123 bp
	R	CTCTCGGGACTCTGAGCACT	
<i>S100</i>	F	GCTTGTCTCTGTGCAAACG	131 bp
	R	TACTTGTAACAAACCGCGA	
<i>Gapdh</i>	F	GAACATCATCCCTGCATCCA	154 bp
	R	GCCAGTGAGCTTCCCGTTCA	

SFI value of nearly 0 represents normal, while an SFI value of – 100 indicates total dysfunction of the sciatic nerve.

EMG

Following 12 weeks of nerve scaffold implantation, EMG evaluation was performed on all rats before sacrifice. Under intraperitoneal xylazine (8 mg/kg) and ketamine hydrochloride (60 mg/kg) anesthesia, the right sciatic nerve of the operated side was re-exposed by longitudinal incision on the posterior aspect of each thigh from the greater trochanter to the knee. A bipolar stimulating electrode was positioned to the nerve trunk at a location 10 mm proximal to the repair site. Compound muscle action potentials (CMAPs) were recorded in the belly of the gastrocnemius muscle at the ipsilateral side using an EMG recorder. The physiologic parameters, including the peak amplitude of compound action potentials and latency, were measured (Bain et al. 1989).

Animal Scarification and Sampling

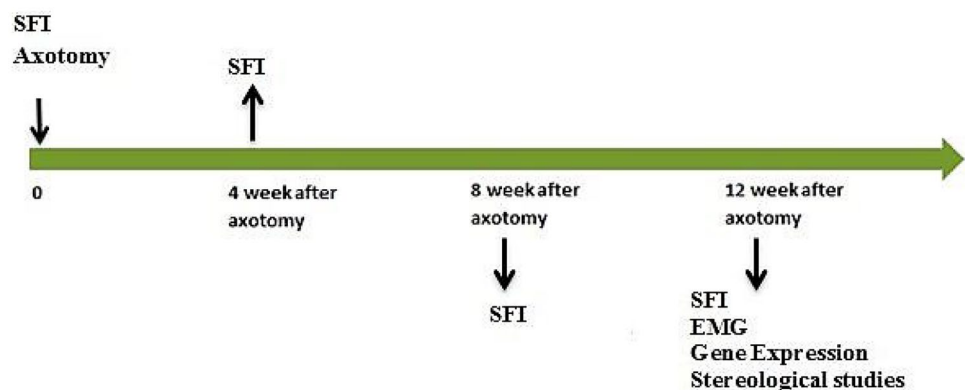
Perfusion and Tissue Collection

After 12 weeks, the animals were anesthetized with ketamine (100 mg/kg) and xylazine (10 mg/kg) intraperitoneally, and then the rats were perfused intracardially with 150 ml normal saline and 200 ml in 4% paraformaldehyde. Sampling

was performed for molecular and histological evaluations. For histological assessments, DRG, spinal cord, and proximal and distal parts of the sciatic nerve were extracted and post-fixed in 4% paraformaldehyde at 48 °C for 4–5 days. The paraffin blocks were prepared and were cut in serial sections of 5- and 10- μ m thickness respectively in order to measure volume, cells, and nerve fiber number, which spinal cord was stained with cresyl violet and DRG, and sciatic nerve was stained respectively with hematoxylin and eosin (H&E) and osmium tetroxide.

RT-PCR

The real-time polymerase chain reaction (RT-PCR) analysis was conducted using specific primers for *brain-derived neurotrophic factor (Bdnf)* and *nerve growth factor (Ngf)* to evaluate the level of neurotrophic factors at the axotomy site. *Schwann100 (S100)* gene expression was also measured as a Schwann cell factor. *Glyceraldehyde-3-phosphate dehydrogenase (Gapdh)* was used as the internal control (Table 1). Reactions were performed using SYBR® Premix Ex Taq™ II (Takara Bio, Inc.) on a Rotor-Gene™ 6000 real-time PCR machine (Corbett Research, Qiagen, Germany). Initial denaturation was performed at 95 °C for 15 min followed by 40 cycles of denaturation at 95 °C for 5 s, under primer-specific conditions (Table 1), and extension at 60 °C for 20 s. Comparative real-time PCR quantitation was conducted between candidate groups using Relative Expression Software Tool

Fig. 1 Schematic timeline of study

(REST) (Pfaffl et al. 2002) (Qiagen). The overall research timeline for the experiments is shown in Fig. 1.

Immunohistochemical Study of GFAP Expression in the Anterior Horn of Spinal Cord

The histological sections from the spinal cord were incubated in primary antibody against *Gfap*, which was diluted (1:300) with PBS containing 0.3% Triton X-100 and 1% bovine serum albumin (BSA) overnight at 4 °C. The sections were then incubated with the avidin–biotin complex substrate and exposed to 0.05% 3,3-diaminobenzidine tetrahydrochloride (DAB) and 0.03% hydrogen peroxide in 0.05 m Tris buffer (pH 7.6). After the immunohistochemical reaction, sections were mounted, counterstained, and observed under a light microscope.

Stereological Estimate of the Total Volume of Spinal Anterior Horn

The volume was estimated using the Cavalieri method. Briefly, 10 sections are selected using systematic, uniformly random sampling (SURS) for stereological estimations. Each microscopic slide was analyzed using a video microscopy system made up of a microscope (E-200, Nikon, Tokyo, Japan) linked to a video camera, a computer, a flat monitor, and a microactuator (MT-12, Heidenhain, Traunreut, Germany). The formula for calculation of the volume of the anterior spinal horn was as follows (Ahmadi et al. 2018; Sladjana et al. 2008; Noorafshan et al. 2014):

$$V_{\text{spinal anterior horn}} = \sum P \times t \times \frac{a}{p} \quad (1)$$

where “ ΣP ” was the total points hitting the anterior horn sections, “ a/p ” was the area associated with each point, and “ t ” was the distance between the sampled sections.

Stereological Estimate of the Number of Neurons, Glial Cells, and Sciatic Nerve Fibers

The optical dissector method was used to determine the total number of neurons, glial cells sciatic nerve fibers. Random sampling was ensured by moving the microscopic field position at equal intervals. A microcator was used to measure the Z-axis movement of the microscope stage. According to the sectional images, an unbiased counting frame with exclusion and inclusion borders was superimposed and observed on the monitor. A nucleus was counted if it fell entirely or partially within the counting frame and did not reach the exclusion line. The numerical density (N_v) was calculated as follows (Noorafshan et al. 2014):

$$N_v = \frac{\Sigma Q}{\Sigma P \times h \times \frac{a}{f}} \times \frac{t}{BA} \quad (2)$$

where ΣQ is the number of the nuclei, h is the height of the disector, a/f is the frame area, ΣP is the total number of the unbiased counting frame in all fields, t is the real section thickness measured in every field using the microcator, and BA is the block advance of the microtome which was set at 10 μm . The total number of neurons, glial cells, and sciatic nerve fibers was estimated by multiplying the N_v 's numerical density (N_v) by the total V .

$$N_{\text{total}} = N_v \times V \quad (3)$$

It should be noted that glial cells are smaller in size than neurons and the nucleolus and cytoplasm of glial cells are not visible.

Stereological Estimate of the Thickness of Myelin Sheath

An average of 10 sections from 10- μm thick sections was randomly selected and studied with 100 \times magnification to estimate the mean thickness of the myelin sheath. The specific line grid (2 parallel lines) was randomly superimposed on the sampled fields to identify measurement sites. The myelin sheath thickness was measured using the orthogonal intercept method, in brief by measuring the length of a line extended perpendicularly from the inner membrane to the outer surface of the myelin sheath at each intercept of the line of the grid with a myelin sheath. It was considered as orthogonal intercept (oi). An average of 100 measurements was made to calculate the harmonic mean thickness using the following formula:

$$T = \frac{\pi}{4} \times L_n \quad (4)$$

The L_n is the means of the intersection points between the axon perimeter and the test lines in this equation.

Data Analysis

The Shapiro–Wilk test determined the distribution of data. Comparing groups were made by one-way analysis of variance (ANOVA), followed by Tukey's multiple comparison test to analyze the difference. Walk data were analyzed using the repeated measures. After repeated measures, differences between curves/groups were determined by the Mann–Whitney test. All statistical works were performed in IBM SPSS version 21. All data are represented as the mean \pm SD. The significance of the comparisons was set at P -value < 0.05 .

Results

BM-MSCs Exhibited Fibroblast-Like Morphology, Multilineage Differentiation Capability and Expression of VEGF Factor

One week after BM cells were cultured, fibroblast-like cells appeared in culture dishes. The cells overgrew and covered the surface (Fig. 2A). Flow cytometry analysis at passage 3 showed that more than 79% of these cells express mesenchymal CD44 and CD90 markers, while only less than 4.3% expressed hematopoietic CD45 and CD34 markers (Fig. 2B). Also, the multilineage differentiation capacity of MSCs into osteogenic and adipogenic lineages was confirmed by Alizarin Red (Fig. 2C) and Oil Red (Fig. 2D) staining, respectively. To examine the ability of purified BM-MSC to produce VEGF factor, we detected these factors by Western blot. Our data revealed that the BM-MSCs could express VEGF (Fig. 2E).

PCL Scaffold Structure

SEM micrographs of the prepared PCL scaffolds are shown in Fig. 3. The nanofibrous microstructure can be seen in these images (Fig. 3A). The incorporation of CM on the fibers is observable in Fig. 3B. According to the results, the plasma treatment following CM coating has no worse effect on the microstructure of the prepared samples, and by the

formation of a thin layer around the fibers, a large surface area of CM would be introduced for the regenerating axons.

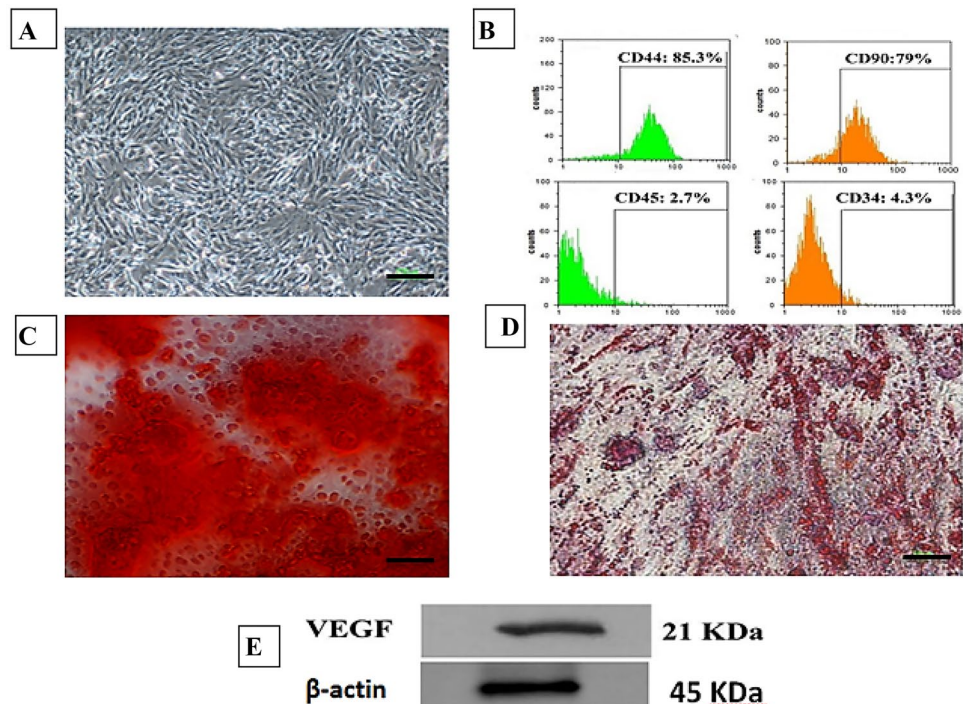
In Vitro Cytotoxicity Evaluation

The probability of the release of cytotoxic materials from the prepared samples was examined via an indirect cytotoxicity test using the L929 mouse fibroblast cell line and MTT assay. Obtained results indicated the complete viability of cells at the exposure with both PCL and CM-coated PCL samples (Fig. 4).

BM-MSC Conditioned Media Loaded on the Scaffold Improved SFI

Walking track analysis was performed to assess the eventual recovery of locomotive function in the experimental rats. At weeks 4, 8, and 12, and before induction of axotomy, SFI values were evaluated. Rats in the axotomy groups showed a time-dependent decrease in SFI values due to sciatic nerve degeneration that was significantly different compared to the control group (P -value < 0.001) (Fig. 5). After 12 weeks, rats engrafted with scaffold and CM-loaded scaffold had significantly less motor impairment when compared with the axotomy group (P -value < 0.01) (Fig. 5). Interestingly, there was a statistically significant difference between the scaffold and CM-loaded scaffold groups at week 12 (P -value < 0.05) (Fig. 5). The SFI values at weeks 4 and 8 were significantly different between the axotomy group with

Fig. 2 Characterization of MSCs. **A** Fibroblast-like morphology of MSCs after 2 weeks of isolation. **B** Flow cytometric analysis at third passage for positive mesenchymal markers (CD44 and CD90), negative hematopoietic (CD34 and CD45). **C** Osteogenic cells showing mineral deposits under osteogenic differentiation medium, stained with Alizarin Red S. **D** Adipogenic cells displaying lipid droplets under adipogenic differentiation medium, stained with Oil Red O. Scale bar = 100 μ m. **E** Expression of VEGF proteins in BMSCs were examined by Western blotting



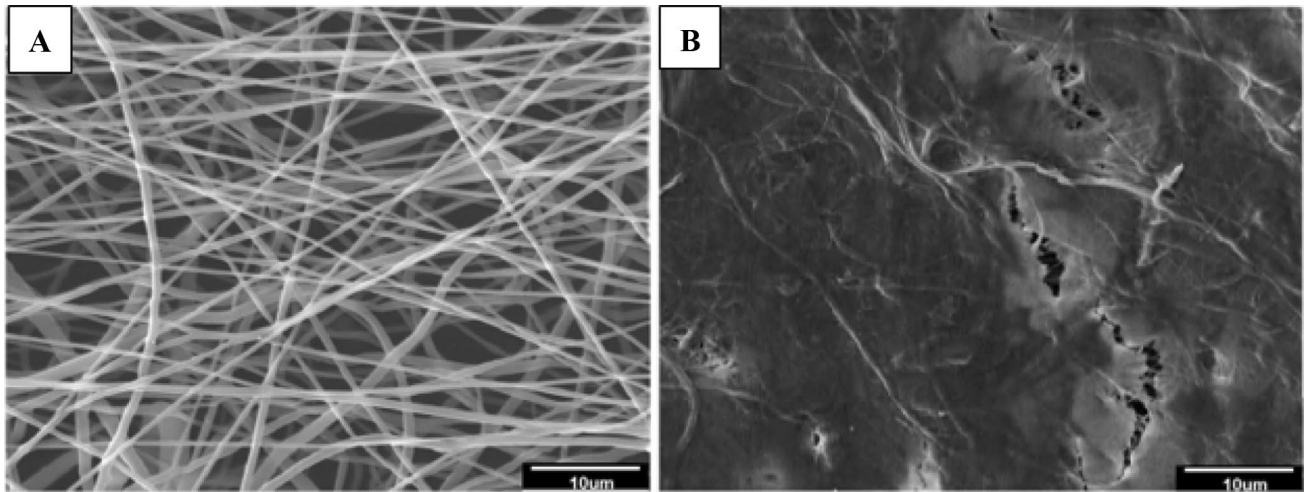


Fig. 3 A, B SEM micrographs of the PCL scaffold before and after CM coating, respectively

scaffold and CM-loaded scaffold groups (P -value < 0.05 and P -value < 0.01), respectively (Fig. 5).

Enhanced Motor Coordination and Muscle Activity Following Engraftment of CM-Loaded Scaffold in Rats After Axotomy

At week 12 post-operation, EMG was used for measuring the effect of CM-loaded scaffold transplantation on muscle activity (Fig. 6A). In this respect, latency implied an enhancement in the scaffold and CM-loaded scaffold groups compared with that in control one ($*P$ -value < 0.05). Following CM-loaded scaffold transplantation, latency also decreased in the treatment group in comparison with that in the scaffold one (P -value < 0.05) (Fig. 6B). Findings

indicated a reduction in the amplitude of the compound muscle action potential (CMAP) in the scaffold and CM-loaded scaffold groups compared with that in control one (P -value < 0.01 and P -value < 0.05 , respectively) (Fig. 6B). However, the amplitude of the CMAP in gastrocnemius muscles had been enhanced after being treated with a CM-loaded scaffold compared to the scaffold group alone (P -value < 0.05) (Fig. 6B).

Total Number of the Nerve Fiber, Thickness of Myelin Sheath of Sciatic Nerves 12 Weeks Post-Surgery

Figure 7 shows the osmic acid images along the cross-sections incised from the segment of the regenerative nerve fibers in different groups following 12 weeks post-surgery. In osmic acid staining, normal nerve presented morphologies of regular nerve fiber alignment, and normal sciatic nerve had dense myelinated nerve fibers with comparatively uniform size and large diameter (Fig. 7(a–d)). The results revealed that the total number of nerve fiber and myelin sheath thickness was a significant reduction in the axotomy groups in comparison to the scaffold (P -value < 0.01), CM-loaded scaffold (P -value < 0.01), and control (P -value < 0.001) groups (Fig. 7B). The nerves recovered from the scaffold and CM-loaded scaffold groups showed the enhanced numbers of the nerve fibers and increased myelin sheath thickness (Fig. 7B) and showed higher remyelination in a group transplanted with scaffold and CM-loaded scaffold. Our results showed that the total number of nerve fiber and myelin sheath thickness was significantly increased in the CM-loaded scaffold groups in comparison to the scaffold groups (P -value < 0.05) (Fig. 7B).

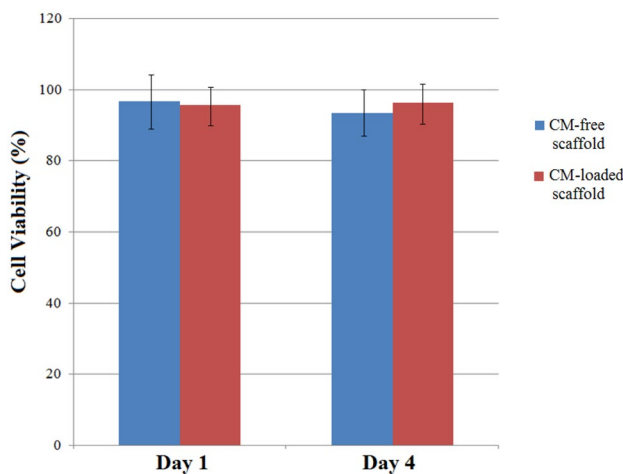
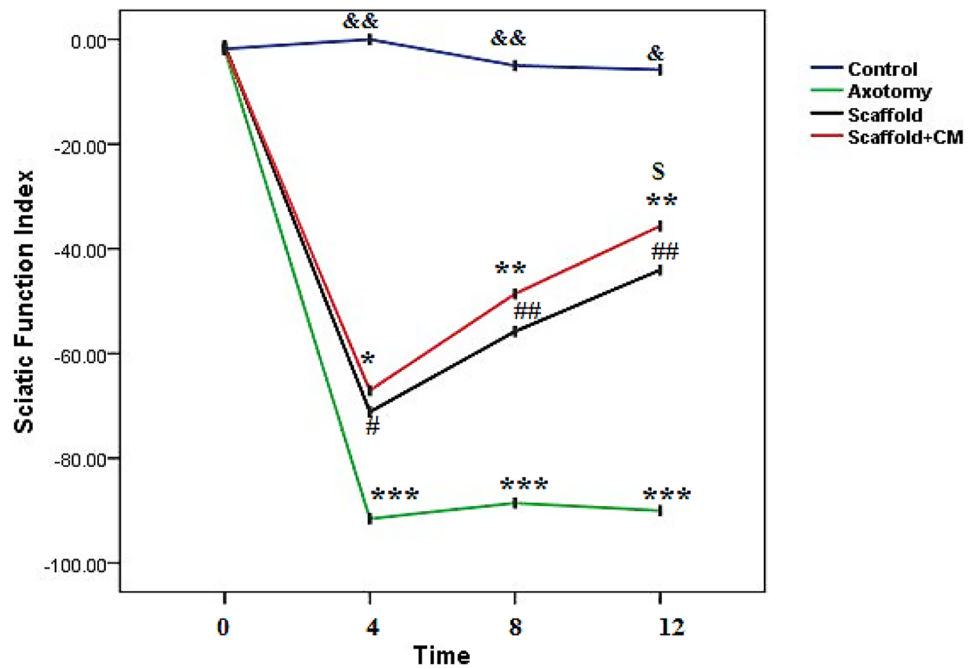


Fig. 4 Cell viability on the prepared sample. Using L929 fibroblasts and MTT staining

Fig. 5 The sciatic functional index (SFI) in all groups. The significant difference between control group with the CM-loaded scaffold and scaffold groups ($^{\$}P < 0.05$, $^{SS}P < 0.01$) is indicated as well as with axotomy group ($^{***}P < 0.001$). The significant difference between axotomy groups with the scaffold + CM ($^{*}P < 0.05$, $^{**}P < 0.01$) and scaffold ($^{\#}P < 0.05$, $^{\#\#}P < 0.01$) groups is indicated. Also, significant differences were shown between scaffold and CM-loaded scaffold groups at week 12 ($^{\$}P < 0.05$)

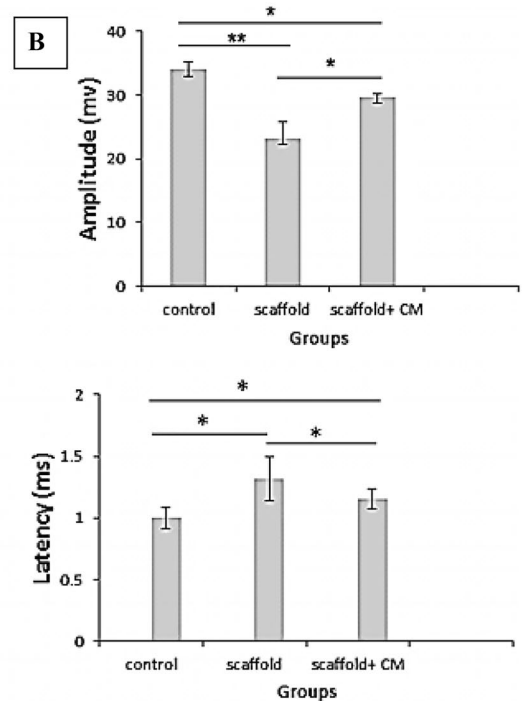
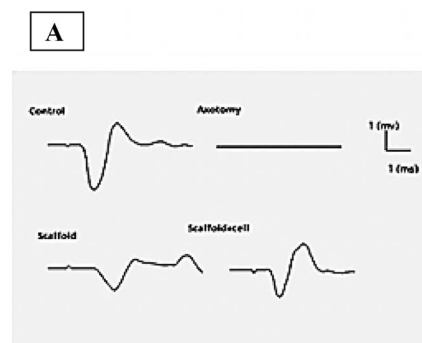


Number of Neuron and Satellite Cells of the DRG

Based on the finding, total numbers of the neurons and satellite cells of the DRG were significantly decreased in the axotomy groups in comparison to the scaffold group (P -value < 0.05), CM-loaded scaffold ($P < 0.01$), and control groups (P -value < 0.01) (Fig. 8). Interestingly, the total

number of neurons and satellite cells of the DRG in the group of CM-loaded scaffold was different with scaffold groups; however, no significant difference between the groups was noted (Fig. 8). Our finding of H&E staining revealed that using the CM-loaded scaffold for bridging 10-mm sciatic nerve deficiencies in the animals could prevent a reduction in the number of neuron and satellite cells of DRG (Fig. 8).

Fig. 6 Muscle activity in rats. **A** The sciatic nerve was stimulated, and the muscle action potential was recorded in the gastrocnemius muscle. **B** EMG amplitude and latency were measured in all groups. Asterisk shows the difference between groups ($^{*}P < 0.05$ and $^{**}P < 0.01$)



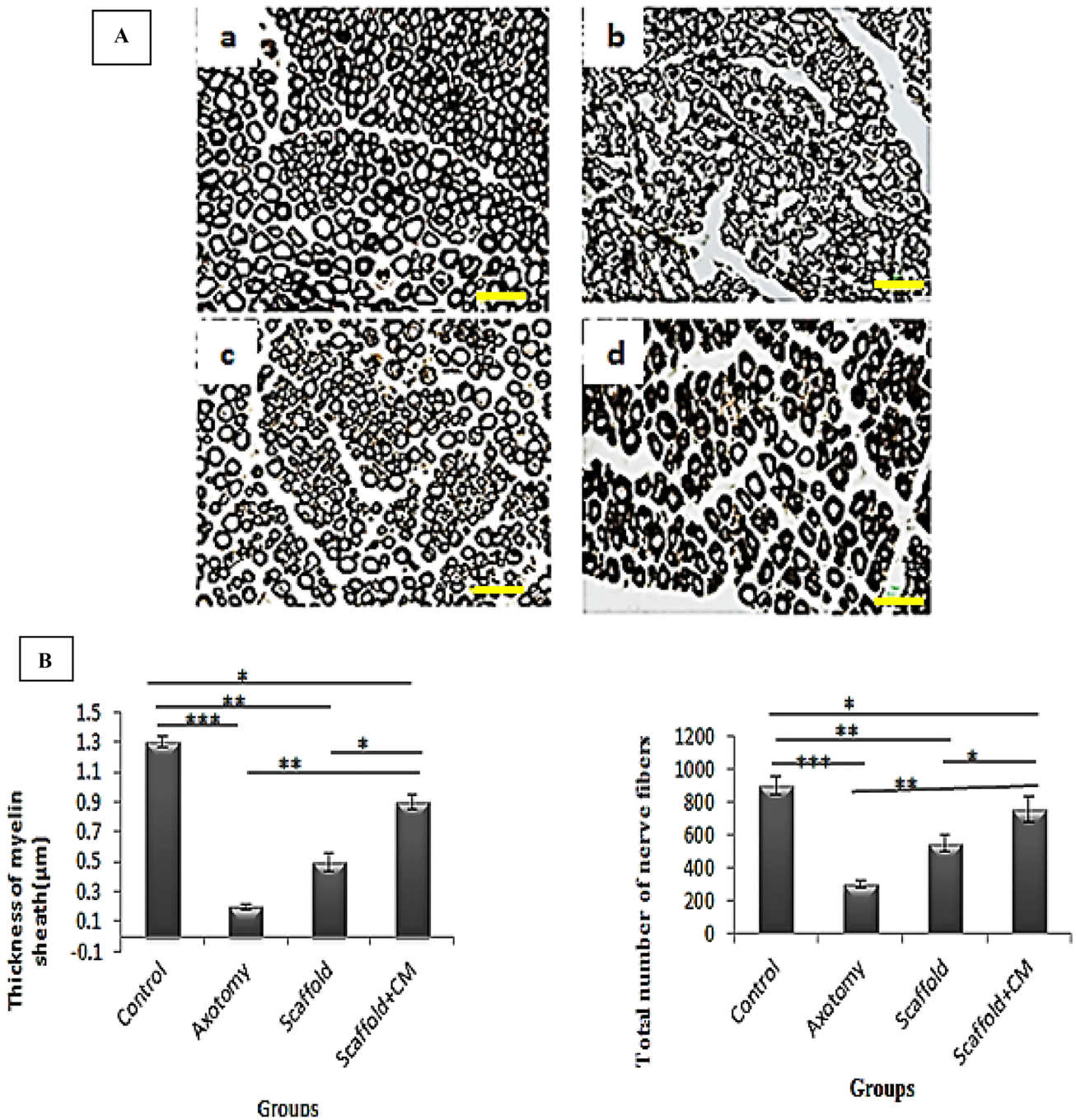


Fig. 7 **A** Histological changes of sciatic nerve. (a) Control, (b) axotomy, (c) scaffold, (d) scaffold +CM, osmium tetroxide staining; bar indicates 10 µm. **B** Histogram of total number of nerve fiber and the thickness of myelin sheath in 4 groups. (* $P < 0.05$, ** $P < 0.01$ and *** $P < 0.001$)

Number of Motoneuron, Neuroglial, and Volume of the Anterior Horn in Spinal Cord

Assessing the anterior horn segments of the spinal cord demonstrated remarkably the decreased number of motoneurons in the axotomy groups in comparison with scaffold (P -value < 0.05), CM-loaded scaffold (P -value < 0.01),

and control groups (P -value < 0.001) (Fig. 9). Our results showed a significant decrease in the number of motor neurons in the scaffold group compared to the CM-loaded scaffold group (P -value < 0.05) (Fig. 9). According to the analysis, the number of neuroglial cells increases in the axotomized rats in comparison with the CM-loaded scaffold (P -value < 0.01) and control groups (P -value < 0.01)

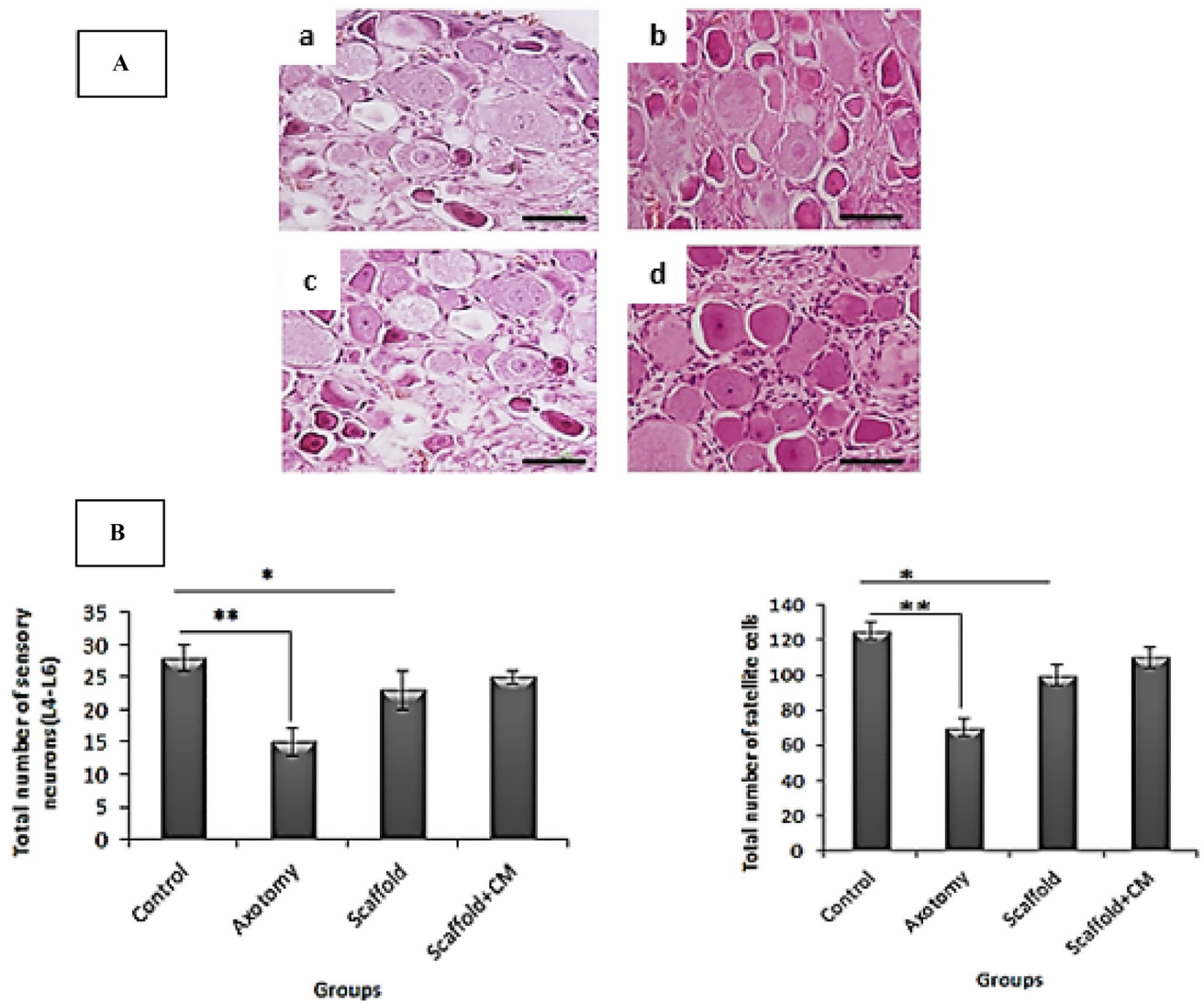


Fig. 8 **A** Transverse sections of DRG observed by light microscopy in the different experimental groups. (a) Control, (b) axotomy, (c) scaffold, (d) scaffold+CM, cresyl violet staining, $\times 10$. Scale

bar = 100 μm . **B** Histogram of total number of sensory neurons and glial cells of DRG (* $P < 0.05$, ** $P < 0.01$)

(Fig. 9). Nonetheless, there is no significant difference between axotomy groups and scaffold groups (Fig. 9). Also, a significant difference between the scaffold while compared with the CM-loaded scaffold groups (P -value < 0.05) was noted (Fig. 9). Based on our results, total volumes of the anterior horn were decreased in the axotomized rats in comparison with control groups (P -value < 0.01) (Fig. 9). Interestingly, the total volumes of anterior horn in the group of axotomy group were different from the CM-loaded scaffold group (P -value < 0.05); no significant difference between the CM-loaded scaffold group compared with the scaffold group (Fig. 9) was observed. The data revealed that using the CM-loaded scaffold for bridging the sciatic nerve deficiencies in the animals could stop the neuron loss, gliosis in the anterior horn of the spinal cord (Fig. 9).

The Expression Level of Astrocytic Marker GFAP

Our results showed the increased expression level of the astrocytic marker *Gfap* in the anterior horn of the spinal cord in the axotomy groups in comparison with the scaffold group (P -value < 0.05), CM-loaded scaffold ($P < 0.01$), and control groups (P -value < 0.001) (Fig. 10). Our results also showed that the *Gfap* positive cells significantly increased the scaffold group compared with the CM-loaded scaffold (P -value < 0.05) and control group (P -value < 0.01) (Fig. 10). However, these findings of immunohistochemistry of astrocytic marker confirmed that astrogliosis was observed in the axotomy groups in comparison to the CM-loaded scaffold, scaffold group, and control groups (Fig. 10).

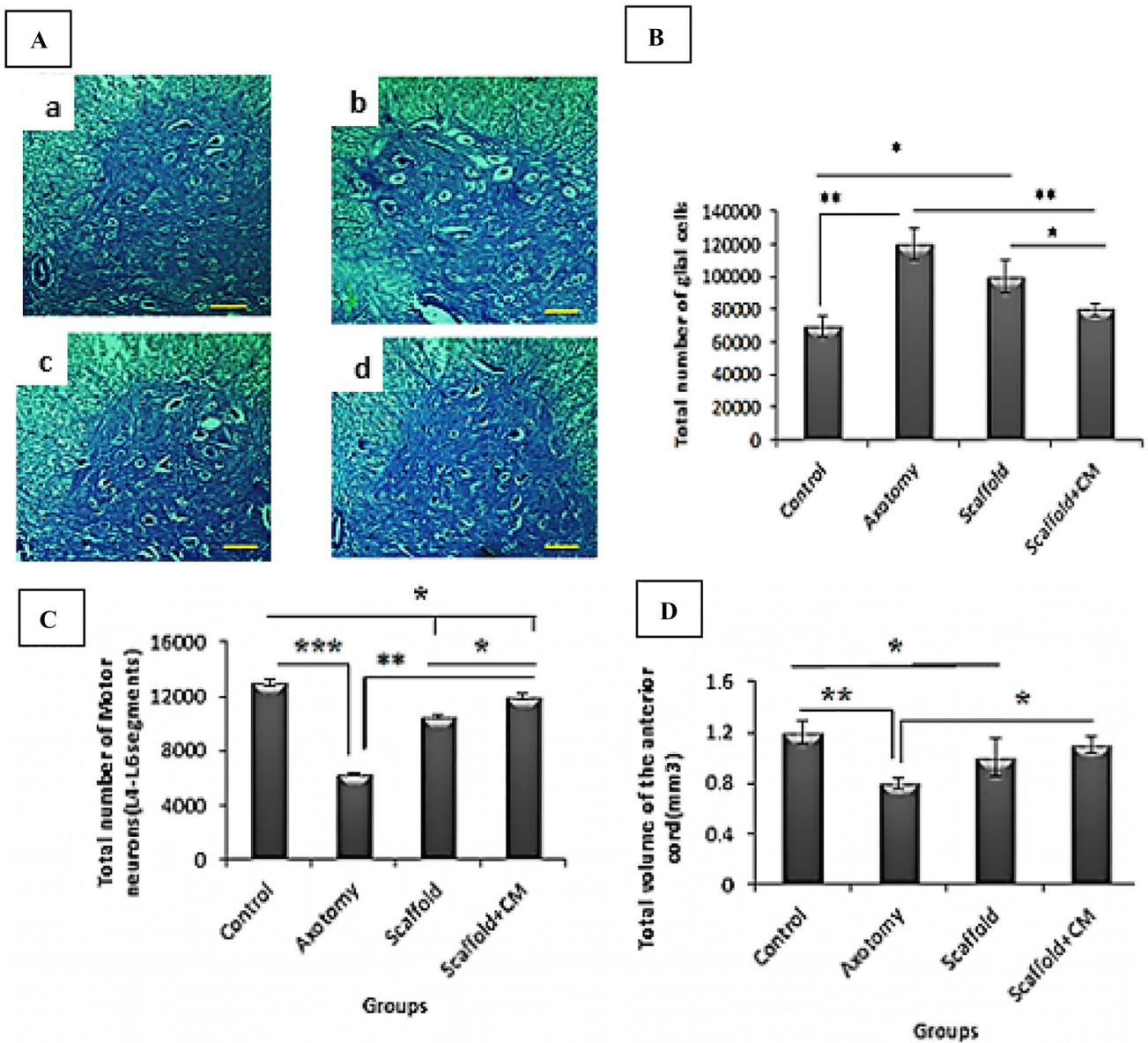


Fig. 9 A Transverse sections of spinal cord observed by light microscopy in the different experimental groups. (a) Control, (b) axotomy, (c) scaffold, (d) scaffold+CM, cresyl violet staining. Scale

bar=100 μm. **B–D** Graphs of total number of motor neurons and glial cells and total volume of anterior horn (* $P < 0.05$, ** $P < 0.01$, and *** $P < 0.001$)

The Increase inNGF, BDNF, and S100 Expression after Engraftment of CM-Loaded Scaffold

In this section, the sciatic nerve determines the gene expression level 12 weeks following the transplantation of the CM-loaded scaffold. According to the real-time PCR analyses (Fig. 11), *Ngf*, *Bdnf*, as well as *S100* expression in the rat’s sciatic nerves downregulated in the axotomy group as compared with the controls (P -value < 0.01) (Fig. 11). Moreover, overexpression in the *Ngf*, *Bdnf*, and *S100* was observed in the scaffold + CM (P -value < 0.01) and scaffold (P -value < 0.05) groups as compared with the

axotomy group. Our results of the level of gene expression in the sciatic nerve tissue were considerably increased in the scaffold + CM group in comparison to the scaffold group (P -value < 0.05) (Fig. 11).

Discussion

Researchers increasingly consider the use of biological materials or synthetic materials such as scaffolds in the form of a nerve conduction channel and/or a bridge at the site of the nerve ending. On the other hand, studies have shown that

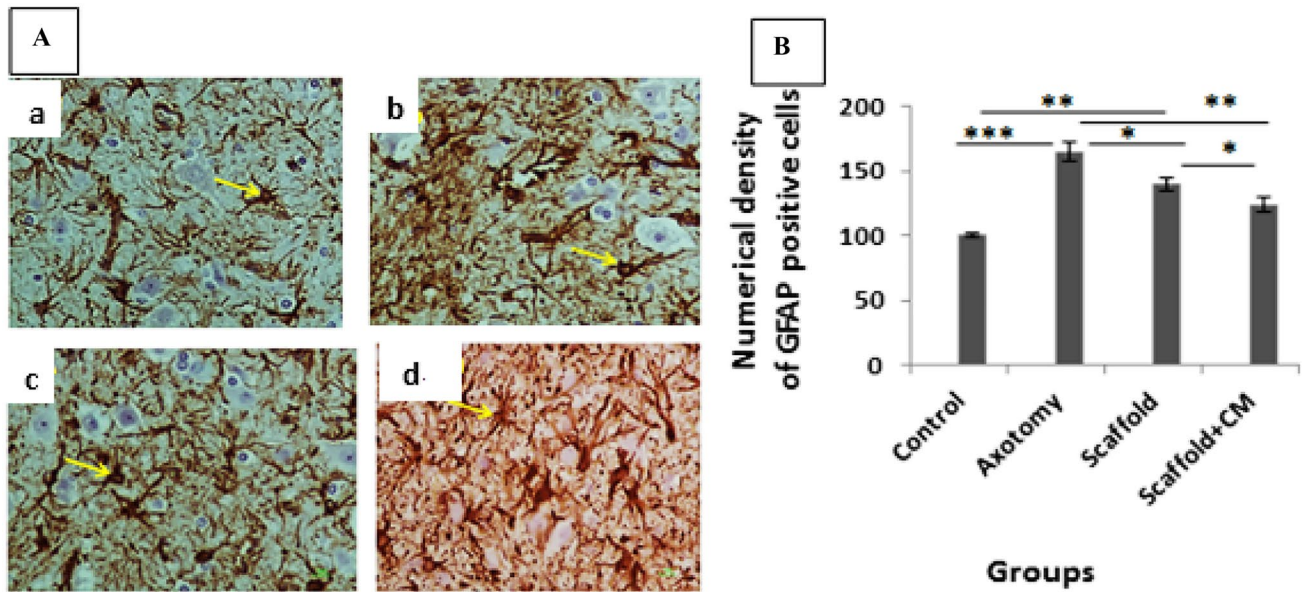


Fig. 10 **A** IHC analysis against GFAP was done among various groups in the anterior horn of spinal cord. $\times 40$. Astrocyte (yellow arrow). **B** Representation of the estimated parameters of the anterior

horn. Numerical density of GFAP positive cells in anterior horn of spinal cord in the different groups is shown. (a) Control, (b) axotomy, (c) scaffold, (d) scaffold + CM ($*P < 0.05$, $**P < 0.01$, $***P < 0.001$)

the use of scaffolds plays a vital role in the migration of glial cells, growth of neurites, and in increasing their survival and proliferation. The sciatica nerve injury results in loss of relative or complete sensory and motor functions (Sladjana et al. 2008; Rodríguez et al. 2004). The use of artificial scaffolds is increasing (Ma 2004) due to their ease of access, flexibility, and reasonable prices. Among these scaffolds, nanofiber scaffolds provide a space like the extracellular matrix for cells by forming a network of permeable fibers with a plurality of pores, affecting the morphology, orientation, adhesion, migration, differentiation, and differentiation function of the cell (Ghasemi-Mobarakeh et al. 2008). Since collagen is a major structural protein of ECM, nanofiber scaffolds are very biocompatible, and therefore these scaffolds are a good candidate for reconstructive medicine (Yang et al. 2008).

Our results demonstrated that the *PCL* scaffold could enhance axonal regeneration and functional recovery, where the results of the SFI test showed that the rats in the scaffold receiving group, along with the CM, can move more quickly. The findings in this study revealed that although the rate of this index was not expected in the experimental group after 12 weeks, there was a significant difference in the results of week 12 in the experimental group receiving the combined usage of CM and *PCL* scaffold compared with the group of axotomy, where sciatic nerve repair is not possible without nerve repair interventions.

Our findings indicated decreases in latency values due to sciatic nerve regeneration in the CM-loaded scaffold group compared with the axotomy group. Furthermore, a

significant difference was observed in the action potential amplitude after sciatic nerve injury in both groups. Compound action potential amplitude was significantly increased in the gastrocnemius muscle of the scaffold + CM group compared to the axotomy group. Studies have shown that the nerve autograft leads to the formation of fibrous tissue and growth restriction for repairing axons (Simões et al. 2010a). The disadvantages of autografts were indicated to be loss of function at the donor site, followed by multiple surgeries. However contradictory reports were raised, where its beneficial effect on axonal regeneration and functional recovery was reported for axonal regeneration and functional recovery (Vargel 2009, Horie et al. 2004). In this study, *PCL* scaffold and BM-*MSC* condition media bridge the gap between the two ends of the nerve to help the growth of the axon.

Recent studies have also attributed a practical application to *MSCs* from BM in regenerating tissue on nanofibrous scaffolds (Shih et al. 2006). Few investigations described the differentiation of *MSC* towards neuronal cells based on the use of electrospun nanofibrous substrates (Xin et al. 2007). *MSCs* have attracted attention due to their potential in transplantation and regeneration therapy of the nervous system and the therapeutic potential for a degenerative and autoimmune disorder that affects the nervous system (Prabhakaran et al. 2009). As indicated, the current study was performed to evaluate the fabrication of a biocompatible nanofibrous scaffold using *MSCs* for neuronal cells, aiming towards a recovery of sciatic nerve injury.

Based on the available data, chitosan/poly (lactic-co-glycolic acid)-based scaffold with bone marrow mesenchymal cells

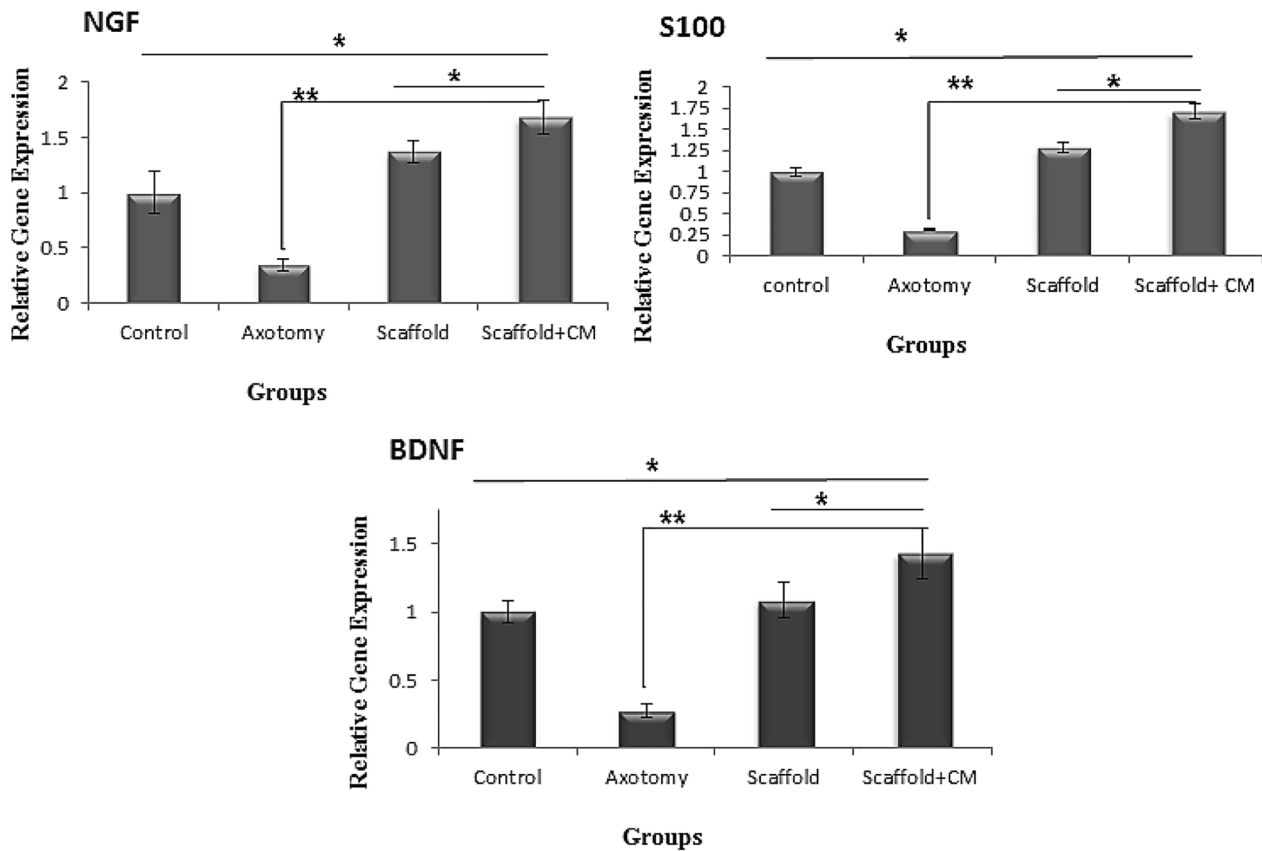


Fig. 11 Relative gene expression measured in the sciatic nerves in different groups with the use of RT-PCR. The significant difference between scaffold groups with axotomy is indicated (* $P < 0.05$, ** $P < 0.01$)

(MSCs) was previously applied for promoting sciatic nerve regeneration and functional recovery in the dog, where its efficacy was achieved after 6 months (Ding et al. 2010). Furthermore, chitosan scaffolds were used to bridge the sciatic nerve gap, where nerve regeneration was observed, and chitosan type III tubulization led to better nerve regeneration and functional recovery than PLGA tubulization control. It is noteworthy that this condition is attributed to the direct effect of scaffolds and the stimulation of Schwann cell proliferation, axon extension, and myelination (Simões et al. 2010b). Rapid repair and regeneration of injured sciatic nerves were demonstrated in rabbits based upon the use of nano-silver-collagen scaffold (Ding et al. 2010). Marinescu et al. examined sciatic nerve repair using collagen–polyvinyl alcohol scaffold and mesenchymal stem cells. They created a 10-mm gap in the sciatic nerve of the rat. After 12 weeks of treatment, histological and immunocytochemistry studies showed that the sciatic nerve was significantly restored (Marinescu et al. 2014). Nevertheless, it is rational to speculate that promoting nerve regeneration and functional recovery can be achieved by incorporating CM into nerve scaffolds.

The results of the stereological study suggested that the sensory neurons of the dorsal root ganglion and the motor neurons of the anterior horn of the spinal cord in the

segment of the sciatic nerve exhibited cell death following nerve damage. After 12 weeks using the conduction channel, the average of the remaining neurons in the treatment group was higher than the axotomy group following nerve repair, and a decrease in neuronal death was observed. It seems that the attachment of proximal and distal parts by using a nerve conduction channel has reduced the death of neurons. The distal segment plays a vital role in neurotrophic factors from the target tissue and Schwann cells by retrograde transfer from the damaged nerve ends (Putchá and Johnson 2004).

Cutting the nerves causes neurons to be deprived of growth factors derived from the target tissue. Neurotrophic factors, by binding to receptors of the tyrosine kinase family, activate a series of intracellular messages that inhibit the activity of pro-apoptotic molecules (Bierlein De la Rosa et al. 2017). Many specific factors were commonly applied for nerve conduit's function, including brain-derived neurotrophic factor (*Bdnf*), nerve growth factor (*Ngf*), and glial-derived nerve growth factor (*Gdnf*) (Pu et al. 1999).

Incorporating CM into nerve scaffolds can achieve good performance to our approach in preventing the death of sensory and motor neurons after sciatic axotomy. In the present study, it was observed that the number of myelinated axons

and the thickness of the myelin sheath increased in the two groups of scaffold and scaffold / CM compared with the nerve axotomy (Pourmohammadi et al. 2012).

The expression levels of NGF and *Bdnf* neurotrophic molecules were investigated using real-time-PCR in the current study. Our findings depicted a significant increase in the expression of these molecules in the CM-loaded PCL and PCL groups compared to the control groups. Neurotrophins are a group of strong factors that regulate the development, survival, flexibility, maintenance, function, and regeneration of neurons in the nervous system. Growth factors are effective in rapid growth and proper routing of recovered axons (Johnson et al. 2008). Many kinds of neurotrophic factors were defined to induce biological actions on sensory neurons. This increase in the expression of neurotrophic factors is related to the physical and chemical characteristics of the CM-loaded PCL scaffold, which has a positive effect on the proliferation and migration of glial cells during axonal repair and increases the neurotrophic factors. The attachment of the proximal and distal parts causes the retrograde transport of released factors from the target tissue and Schwann cells at the attachment site. Growth factors naturally secreted from the Schwann cell and retrograded from the target tissue affect the growth of axons. In addition, the intracanal matrix, like collagen, accelerates axonal regeneration by creating a specific surface for attachment and expansion of growing axons (Prabhakaran et al. 2009).

Target organs of sympathetic and sensory nerves are capable of producing *Ngf* (Barde 1989). In addition, *Ngf* can stimulate neurite outgrowth and increase the survival of sensory ganglia (Ide 1996). *Bdnf* is a neurotrophic factor that is supportively involved in differentiation (Huang and Reichardt 2001) maturation and survival of neurons. The activation of the JAK/STAT pathway in Schwann cells was previously a key mechanism of *Bdnf* increase in nerve regeneration. An increasing body of evidence indicated that BDNF application leads to the production of cytokine Schwann cells, promoting nerve regeneration (Lin et al. 2016). *Bdnf* is involved in enhancing axonal regeneration and promoting axonal sprouting (Lindsay 1988, Boyd and Gordo 2003), while Schwann cells are capable of modulating axonal sprouting via *Bdnf*, resulting in enhancing nerve regeneration (Meyer et al. 1992). Furthermore, the poor recovery of *Bdnf* was rescued by the BMC transplantation, and *Bdnf* from bone marrow-derived cells plays a crucial role in improving the nerve injury (Takemura et al. 2012).

On the other hand, *Vegf* was suggested to promote peripheral nerve regeneration and Schwann cell proliferation of the sciatic nerve and be capable of promoting functional recovery and morphometric indices of the sciatic nerve after transection in the rat (Mohammadi et al. 2013). Based on the

available data, *Vegf* was introduced to improve and alleviate the PNI and effects of lesions in crush models, respectively (Mohammadi et al. 2013; Bischoff et al. 2008). The natural neural scaffolds consisting of *Vegf* were evaluated for repairing a PNI in rats, where recovery is increased. A study mentioned above suggested that short-lived diffusion of growth factors and the guiding of oriented axonal regeneration are two major approaches in promoting peripheral nerve regeneration (Ma et al. 2014).

In the present study, overexpression of the *S100* gene in the CM-loaded PCL and PCL groups was observed in the 12th week. Schwann cells express the *S100* molecules in their cytoplasm. Therefore, this molecule in the peripheral nervous system is considered a marker for Schwann cells. Protein *S100* plays a role in regulating protein phosphorylation, transcription factors, Ca^{2+} homeostasis, the dynamics of cellular structure, enzyme activity, cell growth, cell differentiation, and cellular responses (Chernov et al. 2015).

Regarding the expression of *S100* by Schwann cells and the role of this molecule in growth processes and cellular differentiation and inflammation, it is reasonable to conclude that an increased level of expression of the *S100* gene at the end of the study period indicates nerve repair. It can be stated that when a nerve gets cut, the number of Schwann cells decreases after 3 months if treatment is not done, thereby reducing the expression of the molecule, but the effective treatment caused a significant increase in the number of Schwann cells and expression of *S100* (Patro et al. 2009). At present, the effectiveness of MSC-based therapeutic strategies for PNI can be attributed to paracrine secretion. Various reports explain the role of trophic factors secreted by MSCs toward the repair of damaged tissues. Exosomes have begun to be noticed as a product of paracrine secretion (Tao et al. 2019). Consequently, MSC exosomes may represent a novel therapeutic tool for PNI in subsequent studies.

Conclusion

In the present study, mesenchymal stem cell-derived conditioned medium (CM) was considered an active agent for enhancing nerve regeneration and applied in the sciatic nerve defect site by incorporation into the PCL scaffold composition. Based on the results presented herein, the nerve regeneration achieved by CM-loaded-PCL scaffold was superior to that by the PCL scaffold and other groups. In conclusion, our result indicated that the use of mesenchymal stem cell-derived conditioned medium in the scaffold composition might come through the presence of neurotrophic factors and decreases cell death of neurons and satellite cells. Reduction gliosis leads to accelerating the process of nerve repair.

Acknowledgements This work was performed at the School of Medicine, Shahid Beheshti University of Medical Science.

Declarations

Statement of Ethics The authors declare that all experimental protocols were approved by the Ethics Committee, deputy of research, Shahid Beheshti University of Medical Sciences, Tehran, Iran. All methods were carried out following relevant guidelines and regulations.

Conflict of Interest The authors declare no competing interests.

References

- Ahmadi H, Boroujeni ME, Sadeghi Y, Abdollahifar MA, Khodaghali F, Meftahi GH, Hadipour M, Bayat AH, Shaerzadeh F, Aliaghaei A (2018) Sertoli cells avert neuroinflammation-induced cell death and improve motor function and striatal atrophy in rat model of Huntington disease. *J Mol Neurosci* 65:17–27
- Bain J, Mackinnon S, Hunter D (1989) Functional evaluation of complete sciatic, peroneal, and posterior tibial nerve lesions in the rat. *Plast Reconstr Surg* 83:129–138
- Barde YA (1989) Trophic factors and neuronal survival. *Neuron* 2:1525–1534
- Bierlein Del, Rosa M, Sharma AD, Mallapragada SK, Sakaguchi, DS (2017) Transdifferentiation of brain-derived neurotrophic factor (BDNF)-secreting mesenchymal stem cells significantly enhance BDNF secretion and Schwann cell marker proteins. *J Biosci Biotech* 124:572–582
- Bischoff B, Romstock J, Fahlbusch R, Buchfelder M, Strauss C (2008) Intraoperative brainstem auditory evoked potential pattern and perioperative vasoactive treatment for hearing preservation in vestibular schwannoma surgery. *J Neurol Neurosurg Psychiatry* 79:170–175
- Boyd JG, Gordon T (2003) Glial cell line-derived neurotrophic factor and brain-derived neurotrophic factor sustain the axonal regeneration of chronically axotomized motoneurons in vivo. *Exp Neurol* 183:610–619
- Chernov AV, Dolkas J, Hoang K, Angert M, Srikrishna G, Vogl T, Baranovskaya S, Strongin AY, Shubayev VI (2015) The calcium-binding proteins S100A8 and S100A9 initiate the early inflammatory program in injured peripheral nerves. *J Biol Chem* 290:11771–11784
- Chong EJ, Phan TT, Lim IJ, Zhang Y, Bay BH, Ramakrishna S, Lim CT (2007) Evaluation of electrospun PCL/gelatin nanofibrous scaffold for wound healing and layered dermal reconstitution. *Acta Biomaterialia* 3:321–330
- Ding F, Wu J, Yang Y, Hu W, Zhu Q, Tang X, Liu J, Gu X (2010) Use of tissue-engineered nerve grafts consisting of a chitosan/poly(lactic-co-glycolic acid)-based scaffold included with bone marrow mesenchymal cells for bridging 50-mm dog sciatic nerve gaps. *Tissue Eng Part A* 16:3779–3790
- Ganji R, Piryaeei A, Bayat M, Rajabibazi M, Mohsenifar Z, Kheirjoo R (2014) The effect of human bone marrow-mesenchymal stem cells secretions on diabetic wound healing. *Res Med* 38:10–18
- Ghasemi-Mobarakeh L, Prabhakaran MP, Morshed M, Nasr-Esfahani M-H, Ramakrishna S (2008) Electrospun poly(ϵ -caprolactone)/gelatin nanofibrous scaffolds for nerve tissue engineering. *Biomaterials* 29:4532–4539
- Griffin MD, Ritter T, Mahon BP (2010) Immunological aspects of allogeneic mesenchymal stem cell therapies. *Hum Gene Ther* 21:1641–1655
- Grinsell D, Keating C (2014) Peripheral nerve reconstruction after injury: a review of clinical and experimental therapies. *BioMed Res Int*
- Himes B, Tessler A (1989) Death of some dorsal root ganglion neurons and plasticity of others following sciatic nerve section in adult and neonatal rats. *J Comp Neurol* 284:215–230
- Horie H, Kadoya T, Hikawa N, Sango K, Inoue H, Takeshita K, Asawa R, Hiroi T, Sato M, Yoshioka T (2004) Oxidized galectin-1 stimulates macrophages to promote axonal regeneration in peripheral nerves after axotomy. *J Neurosci* 24:1873–1880
- Huang EJ, Reichardt LF (2001) Neurotrophins: roles in neuronal development and function. *Annu Rev Neurosci* 24:677–736
- IDE C (1996) Peripheral nerve regeneration. *Neurosci Res* 25:101–121
- Johnson EO, Charchanti A, Soucacos PN (2008) Nerve repair: experimental and clinical evaluation of neurotrophic factors in peripheral nerve regeneration. *Injury* 39(Suppl 3):S37–42
- Karaoz E, Aksoy A, Ayhan S, Sarıboyacı AE, Kaymaz F, Kasap M (2009) Characterization of mesenchymal stem cells from rat bone marrow: ultrastructural properties, differentiation potential and immunophenotypic markers. *Histochem Cell Biol* 132:533
- Kim CH, Khil MS, Kim HY, Lee HU, Jahng KY (2006a) An improved hydrophilicity via electrospinning for enhanced cell attachment and proliferation. *J Biomed Mater Res Part b: Appl Biomater: an Official Journal of the Society for Biomaterials, the Japanese Society for Biomaterials, and the Australian Society for Biomaterials and the Korean Society for Biomaterials* 78:283–290
- Kim CH, Khil MS, Kim HY, Lee HU, Jahng KY (2006b) An improved hydrophilicity via electrospinning for enhanced cell attachment and proliferation. *J Biomed Mater Res B Appl Biomater* 78:283–290
- Koh H, Yong T, Chan C, Ramakrishna S (2008) Enhancement of neurite outgrowth using nano-structured scaffolds coupled with laminin. *Biomaterials* 29:3574–3582
- Ladak A, Olson J, Tredget E, Gordon T (2011) Differentiation of mesenchymal stem cells to support peripheral nerve regeneration in a rat model. *Exp Neurol* 228:242–252
- Lee CH, Shin HJ, Cho IH, Kang YM, Kim IA, Park KD, Shin JW (2005) Nanofiber alignment and direction of mechanical strain affect the ECM production of human ACL fibroblast. *Biomaterials* 26:1261–1270
- Li WJ, Cooper Jr JA, Mauck RL, Tuan RS (2006) Fabrication and characterization of six electrospun poly(α -hydroxy ester)-based fibrous scaffolds for tissue engineering applications. *Acta Biomaterialia* 2:377–385
- Lin G, Zhang H, Sun F, Lu Z, Reed-Maldonado A, Lee YC, Wang G, Banie L, Lue TF (2016) Brain-derived neurotrophic factor promotes nerve regeneration by activating the JAK/STAT pathway in Schwann cells. *Transl Androl Urol* 5:167–175
- Lindsay RM (1988) Nerve growth factors (NGF, BDNF) enhance axonal regeneration but are not required for survival of adult sensory neurons. *J Neurosci* 8:2394–2405
- Ma F, Xiao Z, Meng D, Hou X, Zhu J, Dai J, Xu R (2014) Use of natural neural scaffolds consisting of engineered vascular endothelial growth factor immobilized on ordered collagen fibers filled in a collagen tube for peripheral nerve regeneration in rats. *Int J Mol Sci* 15:18593–18609
- Ma PX (2004) Scaffolds for tissue fabrication. *Materials Today* 7:30–40
- Marinescu SA, Zărnescu O, Mihai IR, Giuglea C, Sinescu RD (2014) An animal model of peripheral nerve regeneration after the application of a collagen-polyvinyl alcohol scaffold and mesenchymal stem cells. *Rom J Morphol Embryol* 55:891–903
- Meyer M, Matsuoka I, Wetmore C, Olson L, Thoenen H (1992) Enhanced synthesis of brain-derived neurotrophic factor in the lesioned peripheral nerve: different mechanisms are responsible for the regulation of BDNF and NGF mRNA. *J Cell Biol* 119:45–54

- Mohammadi R, Ahsan S, Masoumi M, Amini K (2013) Vascular endothelial growth factor promotes peripheral nerve regeneration after sciatic nerve transection in rat. *Chin J Traumatol* 16:323–329
- Morales MM (2007) Terapias avançadas: células-tronco, terapia gênica e nanotecnologia aplicada à saúde. Sang WH. Introdução. História da terapia gênica, estado da arte, técnicas e ética. São Paulo: Atheneu, 105–25
- Noorafshan A, Abdollahifar MA, Asadi-Golshan R, Rashidian-Rashidabadi A, Karbalay-Doust S (2014) Curcumin and sertraline prevent the reduction of the number of neurons and glial cells and the volume of rats' medial prefrontal cortex induced by stress. *Acta Neurobiol Exp (wars)* 74:44–53
- Patro N, Shrivastava M, Tripathi S, Patro IK (2009) S100 β upregulation: A possible mechanism of deltamethrin toxicity and motor coordination deficits. *Neurotoxicol Teratol* 31:169–176
- Pfaffl MW, Horgan GW, Dempfle L (2002) Relative expression software tool (REST) for group-wise comparison and statistical analysis of relative expression results in real-time PCR. *NAR* 30:e36
- Pierucci A, de Oliveira ALR (2006) Increased sensory neuron apoptotic death 2 weeks after peripheral axotomy in C57BL/6J mice compared to A/J mice. *Neurosci Lett* 396:127–131
- Pittenger MF, Mackay AM, Beck SC, Jaiswal RK, Douglas R, Mosca JD, Moorman MA, Simonetti DW, Craig S, Marshak DR (1999) Multilineage potential of adult human mesenchymal stem cells. *Science* 284:143–147
- Pourmohammadi N, Alimoradi H, Mehr SE, Hassanzadeh G, Hadian MR, Sharifzadeh M, Bakhtiarian A, Dehpour AR (2012) Lithium attenuates peripheral neuropathy induced by paclitaxel in rats. *Basic Clin Pharmacol Toxicol* 110:231–237
- Prabhakaran MP, Venugopal JR, Ramakrishna S (2009) Mesenchymal stem cell differentiation to neuronal cells on electrospun nanofibrous substrates for nerve tissue engineering. *Biomaterials* 30:4996–5003
- Pu LL, Syed SA, Reid M, Patwa H, Goldstein JM, Forman DL, Thomson JG (1999) Effects of nerve growth factor on nerve regeneration through a vein graft across a gap. *Plast Reconstr Surg* 104:1379–1385
- Putchá GV, Johnson EM (2004) 'Men are but worms:' neuronal cell death in *C. elegans* and vertebrates. *Cell Death Differ* 11:38–48
- Rodríguez FJ, Valero-Cabre A, Navarro X (2004) Regeneration and functional recovery following peripheral nerve injury. *Drug Discov Today: Dis Models* 1:177–185
- Schnell E, Klinkhammer K, Balzer S, Brook G, Klee D, Dalton P, Mey J (2007) Guidance of glial cell migration and axonal growth on electrospun nanofibers of poly-epsilon-caprolactone and a collagen/poly-epsilon-caprolactone blend. *Biomaterials* 28:3012–3025
- Shih YR, Chen CN, Tsai SW, Wang YJ, Lee OK (2006) Growth of mesenchymal stem cells on electrospun type I collagen nanofibers. *Stem Cells* 24:2391–2397
- Siemionow M, Brzezicki G (2009) Current techniques and concepts in peripheral nerve repair. *Int Rev Neurobiol* 87:141–172
- Simões MJ, Amado S, Gärtner A, Armada-Da-Silva PA, Raimondo S, Vieira M, Luís AL, Shirosaki Y, Veloso AP, Santos JD (2010) Use of chitosan scaffolds for repairing rat sciatic nerve defects. *Ital J Anat Embryol* 115:190
- Simões MJ, Amado S, Raimondo S, Armada-Da-Silva PAS, Gärtner A (2010b) Use of chitosan scaffolds for repairing rat sciatic nerve defects. <http://digital.casalini.it/2490996>
- Sladjana UZ, Ivan JD, Bratislav SD (2008) Microanatomical structure of the human sciatic nerve. *Surg Radiol Anat* 30:619–626
- Takemura Y, Imai S, Kojima H, Katagi M, Yamakawa I, Kasahara T, Urabe H, Terashima T, Yasuda H, Chan L, Kimura H, Matsusue Y (2012) Brain-derived neurotrophic factor from bone marrow-derived cells promotes post-injury repair of peripheral nerve. *PLoS One* 7, e44592
- Tao SC, Guo SC, Collett J (2019) A novel role for extracellular vesicles in cytopathology and new therapeutic strategies. *Biomed Res Int* 2019:7137613
- Terenghi G (1999) Peripheral nerve regeneration and neurotrophic factors. *J Anat* 194:1–14
- Vargel I (2009) Impact of vascularization type on peripheral nerve microstructure. *J Reconstr Microsurg* 25:243–253
- Vestergaard S, Tandrup T, Jakobsen J (1997) Effect of permanent axotomy on number and volume of dorsal root ganglion cell bodies. *J Comp Neurol* 388:307–312
- Wright KT, Masri WE, Osman A, Chowdhury J, Johnson WE (2011) Concise review: bone marrow for the treatment of spinal cord injury: mechanisms and clinical applications. *Stem Cells* 29:169–178
- Xin X, Hussain M, Mao JJ (2007) Continuing differentiation of human mesenchymal stem cells and induced chondrogenic and osteogenic lineages in electrospun PLGA nanofiber scaffold. *Biomaterials* 28:316–325
- Yang L, Fitie CF, van der Werf KO, Bennink ML, Dijkstra PJ, Feijen J (2008) Mechanical properties of single electrospun collagen type I fibers. *Biomaterials* 962–955:29
- Zalewski AA, Gulati AK (1981) Rejection of nerve allografts after cessation of immunosuppression with cyclosporin A. *Transplantation* 31:88

Publisher's Note Springer Nature remains neutral with regard to jurisdictional claims in published maps and institutional affiliations.